

Throughput/Delay Measurements of Limited Feedback Beamforming in Indoor Wireless Networks

Robert C. Daniels, Ketan Mandke, Kien T. Truong, Scott M. Nettles, and Robert W. Heath, Jr.

Wireless Networking and Communications Group

The University of Texas at Austin

1 University Station, Mail Code: C0806, Austin, TX 78712

Abstract—This paper investigates the tradeoff between throughput and feedback delay of limited feedback beamforming in indoor wireless channels with a practical MIMO-OFDM prototype. Past descriptions of this tradeoff are largely based on simplified models of the wireless channel. Unfortunately, wireless channel models may not accurately represent the complexities of a real wireless channel. Furthermore, system impairments, including channel estimation error, only exacerbate the problem of modeling a real wireless system. One such analytical result predicts the performance of limited feedback beamforming as an exponential function of feedback delay. This analytical result has been confirmed through Monte Carlo simulation under Rayleigh fading channel models. Through rigorous measurements and experimentation this paper both evaluates the performance of limited feedback beamforming under feedback delay and confirms the accuracy of the analytical results.

I. INTRODUCTION

Multiple-input multiple-output (MIMO) wireless systems employ multiple antennas at both the transmitter and the receiver to offer higher data throughput and reliability than single-antenna links. By aligning the transmitted signal with the dominant eigenmode of the MIMO channel matrix, beamforming techniques allow MIMO systems to obtain full diversity order and improve the bit-error-rate (BER) [1]. Beamforming requires the availability of channel state information at the transmitter. In the absence of perfect channel knowledge at the transmitter, the CSI can be quantized at the receiver and sent back to the transmitter using a low-rate feedback channel [2]. This technique is known as *limited feedback*. Different types of limited feedback for beamforming have been developed [3]–[5]. It was also shown that limited feedback beamforming systems with only 5 or 6 feedback bits exhibit performance very close to unquantized beamforming systems [3], [6].

Most prior work on limited feedback beamforming assumes that the feedback channel is zero-delay such that instantaneous CSI can be delivered to the transmitter. In practical systems, however, the existence of feedback delay is inevitable due to signal processing and transmission delays. Because of the time-varying nature of the wireless channel, feedback delay can cause a mismatch between CSI at the transmitter and the actual channel state. In other words, feedback delay decreases the performance of limited feedback beamforming systems.

This material is based in part upon work supported by the National Science Foundation under grants CCF-514194 and CNS-626797, the Air Force Research Lab under grant numbers FA8750-06-1-0091 and FA8750-05-1-0246, and the DARPA IT-MANET program, Grant W911NF-07-1-0028.

Analytical results and measurements have characterized the performance degradation of feedback delay in beamforming [7]–[10]. Unfortunately these results make specific assumptions about the channel model. Recent work has shown a more general Markov model to characterize capacity loss due to feedback delay with limited feedback beamforming [11]. This paper, through exhaustive measurements of throughput (goodput) to approximate capacity, confirms this analytical result for predicting the observed effects of feedback delay. We not only verify, but also show that simple measurements can characterize the feedback delay tradeoff, thus avoiding extensive measurement campaigns as conducted in this paper. The use of Hydra, a flexible, software-defined wireless prototype, is a valuable new measurement apparatus that considerably reduced the complexity of the substantial experiments performed in this paper through a programmable physical layer.

Notation: A random variable $X \in [a, b]$ with uniform distribution is denoted $X \sim \mathcal{U}[a, b]$. The transpose of matrix \mathbf{A} is labeled \mathbf{A}^T and the Hermitian transpose is given by \mathbf{A}^H . Row x or column y of matrix \mathbf{A} is specified by $[\mathbf{A}]_{x,:}$ or $[\mathbf{A}]_{:,y}$, respectively. Similarly, the entry of matrix \mathbf{A} at row x and column y is stated as $[\mathbf{A}]_{x,y}$. Finally, adopting engineering notation, $j = \sqrt{-1}$.

II. SYSTEM DESCRIPTION

All limited feedback beamforming experiments in this paper were conducted on the Hydra MIMO-OFDM multihop network prototype at the University of Texas at Austin. The reader is encouraged to see [12]–[14] for a more detailed discussion of Hydra.

A. RF/Baseband Hardware Specification

Table I lists the relevant characteristics of the Hydra system hardware for the experiments in this paper. The operating frequency was placed at the upper edge of the 2.45 GHz industrial, scientific, and medical (ISM) band, above all interference observed by the spectrum analyzer during the experiment [12]. The choice of this frequency is relevant to IEEE 802.11n wireless LANs that will soon occupy this spectrum with beamforming-capable physical layers. For this experiment, the bandwidth is not of considerable importance since, with the exception of ultrawideband (UWB) channels, coherence time statistics are not dependent on the bandwidth of operation [15]. The maximum transmit power is listed as 10 mW, but in order to maintain linearity at the transmitter, typical operation

TABLE I
RF/BASEBAND HARDWARE SPECIFICATION FOR EXPERIMENTS

Specification	Value
Operating Frequency	2.5 GHz
Maximum Transmit Power	10 mW
Symbol Rate	1 MHz [†]
Antenna Type	L-shaped Microstrip
Antenna Reflection Coefficient	< -20 dB
Number of Receive Antennas	2
Number of Transmit Antennas	2

[†] Although the USRP supports 20 MHz sampling rates, the bandwidth is constrained by the USB 2.0 interface.

was below 7.5 mW. Custom L-shaped copper microstrip antennas were chosen over off-the-shelf commercial WLAN antenna products because of their desirable S_{11} reflection coefficient characteristics, which fell below -20 dB for the entire spectrum of operation.

B. Software Architecture

Hydra features a completely software-defined protocol architecture that runs on a general purpose processor. The physical layer code is implemented using GNU Radio. This open-source software allows developers to implement modular signal processing blocks in C++ and flexibly connect them together using python as a glue language.

C. Physical Layer Algorithms

Hydra follows the IEEE 802.11 MIMO-OFDM PHY as provided by *Task Group N* in its Draft 2.0 Standard [16]. The orthogonal frequency division multiplexing (OFDM) modulation in this physical layer provides efficient equalization of frequency selective fading. Moreover, the MIMO algorithms in the standard allow for a framework to perform space-time processing techniques along with feedback functionality. Both of these features along with all the components found in traditional PHYs, make its implementation desirable for commercial products and experimentation alike. This physical layer simplified the design process considerably for the experiments in this paper.

Conforming with the 802.11n physical layer, blocks of binary data, that we shall denote *packets*, are transmitted inside a *frame*. This frame format, as illustrated in Figure 1 (a), serves many purposes. First, the training sequences in the packet allow for asynchronous frame detection. Second, the training sequences allow for measurement of impairments, such as frequency offset, and relevant parameters, such as the wireless channel impulse response for channel equalization. The data payload is a waveform expression of the binary packet. The parameters used to map the binary packet to a continuous waveform are encoded in the header of the frame.

The only non-standard component used in this experiment is the Extended Training. As mentioned earlier, the training sequences in the frame can be used for channel impulse response estimation. This is necessary to perform proper equalization of the distortion effects of the wireless channel. Unfortunately, transmission schemes, such as beamforming,

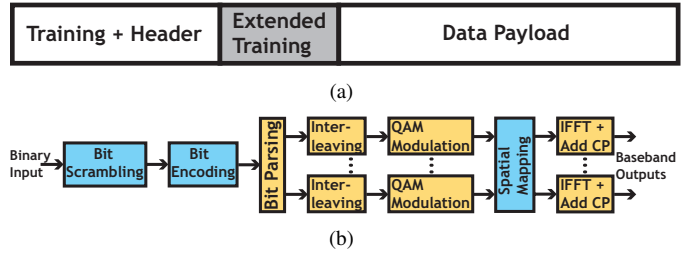


Fig. 1. IEEE 802.11n frame format (a) and transmit processing (b)

become part of the *effective* wireless channel. That means that CSI feedback from channel estimates of this training no longer represent the channel of interest, but a beamformed version of that channel. The 802.11n standard provides a method for extracting the true channel from the beamformed version of the channel. Preferring simplicity over efficiency, Hydra was designed so that extra training information was sent in each frame without any beamforming, or more generally (as we shall see later) without spatial mapping. In the experiments, the Extended Training field provided the CSI feedback as well as the non-beamformed SNR estimates for comparing beamforming and cyclic delay diversity.

The structure of the 802.11n PHY transmitter, as implemented in Hydra, is shown in Figure 1 (b). For the purposes of constructing a mathematical system model of the experiments, the key component of the transmission structure is the spatial mapping block. Let $\mathbf{x}_k^{l,m} = [x_{1,k}^{l,m}, x_{2,k}^{l,m}, \dots, x_{N_{STS,k}}^{l,m}]^T$ represent the input to the spatial mapping block where $x_{i,k}^{l,m} \in \mathbb{C}$, for the k th subcarrier of the l th OFDM symbol in packet m , and N_{STS} is the number of space-time-streams (or distinct streams) in the MIMO signal. Since the main function of the system model is for representation of the transmission strategies, the actual OFDM symbol and packet specified are irrelevant. In other words, the system model holds *equally* for all OFDM symbols in all packets. Therefore, the l,m notation is dropped and $x_{i,k}^{l,m} = x_{i,k}$ for the remainder of the paper. The spatial mapping function $s(\bullet)$ maps the complex vector of dimension N_{STS} to a complex vector of dimension N_{TX} , $s : \mathbb{C}^{N_{STS}} \rightarrow \mathbb{C}^{N_{TX}}$, where N_{TX} is the number of transmit antennas. Given that the feedback transmission strategies will not include spatial multiplexing or space-time block coding, it can be assumed throughout the remainder of this paper that $N_{STS} = 1 \Rightarrow \mathbf{x}_k = x_{1,k} \triangleq x_k$. Furthermore, the spatial mapping function is restricted to the space of linear functions such that $s(\mathbf{x}_k)$ represents a matrix transformation. In other words, $s(\mathbf{x}_k) = \mathbf{Q}_k \mathbf{x}_k = \mathbf{q}_k x_k = \tilde{\mathbf{x}}_k$, where $\tilde{\mathbf{x}}_k$ is the spatially mapped output and $\mathbf{Q}_k \in \mathbb{C}^{N_{TX} \times N_{STS}}$ is the spatial mapping matrix. Several transmit diversity strategies can be packaged into this matrix framework, including digital beamforming (BF) and cyclic delay diversity (CDD) [17], both of which will be revisited after the Hydra receiver is discussed.

The receiver structure is displayed in Figure 2. Like the transmitter, the key component of the receiver involves spatial mapping, in this case extracting an estimate $\hat{\mathbf{x}}_k$ of the k th

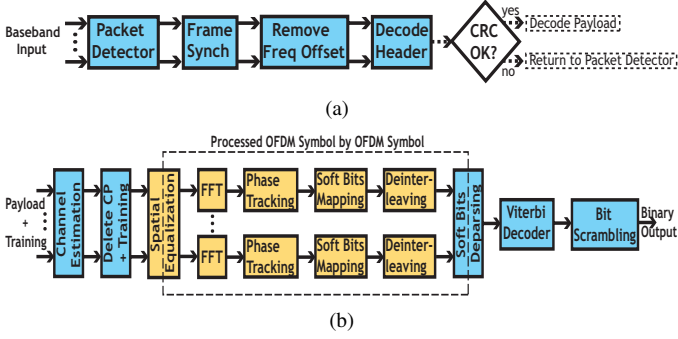


Fig. 2. Hydra receiver synchronization (a) and data processing (b)

subcarrier in each OFDM symbol. This estimate of \mathbf{x}_k follows the combination of the spatial equalization and FFT blocks in Figure 1. If frequency domain equalization is performed, this obviates the need for an explicit FFT operation after the spatial equalization. In a sense, the Spatial Equalization block is the inversion of the combination of the wireless channel and the spatial mapping block. It is assumed that, by using OFDM, the wireless channel impulse response experienced by each subcarrier is frequency flat. Additionally, the model assumes that the coherence time of the wireless channel impulse response is large enough such that each packet observes a constant channel over the duration of waveform transmission. Both of these assumptions are often accepted for indoor channels [15]. Hence, let $\mathbf{H}_k \in \mathbb{C}^{N_{RX} \times N_{TX}}$ represent the complex baseband frequency flat impulse response of the wireless channel for OFDM subcarrier k . Effectively, the spatial equalization block receives \mathbf{y}_k and maps it with function $r(\bullet)$ to $\hat{\mathbf{x}}_k$. If we also assume that the receiver is linear, then $r(\mathbf{y}_k) = \mathbf{G}_k^H \mathbf{y}_k = \mathbf{g}_k^H \mathbf{y}_k$, where $\mathbf{G}_k \in \mathbb{C}^{N_{RX} \times N_{STS}}$. Note again that $\hat{\mathbf{x}}_k = \hat{x}_{1,k} = \hat{x}_k$ since $N_{STS} = 1$. It is now possible to create the complex baseband system model representing the input and output of the effective channel (combined spatial mapping and wireless channel). Thus,

$$\hat{x}_k = (\mathbf{g}_k^H \mathbf{H}_k \mathbf{q}_k) x_k \quad (1)$$

may be used to represent cyclic delay diversity, digital beamforming, limited-feedback beamforming and equalization methods.

Cyclic delay diversity is a simple, yet effective method for achieving full diversity order without knowledge of the wireless channel impulse response at the transmitter. By applying a discrete-time, per-transmit-antenna circular shift to each OFDM symbol it is possible to translate the spatial diversity experienced by multiple transmit antennas into frequency diversity. For bit-interleaved and coded OFDM systems, see Figures 1 and 2, the forward error correction over the subcarriers captures the frequency diversity created in the wireless channel. OFDM symbols preserve the properties of the discrete Fourier transform (DFT) by adding a cyclic prefix. It follows that the spatial mapping vector of cyclic delay diversity, for each scalar element of \mathbf{q}_k^{CDD} ,

$$q_{i,k}^{CDD} \triangleq \exp \left\{ \frac{-j2\pi k N_{i,CS}}{N_{DFT}} \right\} \quad (2)$$

where N_{DFT} is the block size of the DFT and $N_{i,CS}$ is the number of discrete-time symbols to be circularly shifted on transmit antenna i [18].

Digital beamforming, using channel state information feedback, attempts to transmit all of the energy over the maximum eigenmode of the effective channel $\mathbf{g}_k^H \mathbf{H}_k \mathbf{q}_k$. The optimal beamforming solution, in terms of maximizing the effective channel total energy, follows from the singular value decomposition of the channel matrix, $\mathbf{H}_k = \mathbf{U}_k \mathbf{S}_k \mathbf{V}_k^H$, where \mathbf{U}_k and \mathbf{V}_k are unitary matrices and \mathbf{S}_k is a diagonal matrix of dimension $\min\{N_{TX}, N_{RX}\}$. Hence, assuming the diagonal elements of \mathbf{S}_k are sorted by descending amplitude, the optimal beamforming vector is

$$\mathbf{q}_k^{BF} \triangleq [\mathbf{V}_k]_{:,1} \quad (3)$$

and the corresponding optimal combining vector

$$(\mathbf{g}_k^{BF})^H \triangleq [\mathbf{U}_k^H]_{1,:} \quad (4)$$

provides the maximum energy effective channel response. Note that vectors (3) and (4) are not unique and remain optimal for any scalars $e^{j\phi}$ and $e^{-j\phi}$, respectively, for $\phi \in \mathbb{R}$.

Limited feedback beamforming reduces the overhead of transmitting the complete CSI over the feedback channel. By creating finite-size codebooks with a specified bit-precision, feedback can drastically be reduced using the beamforming codeword index instead of the codeword itself. There exist several ways to construct the codebook including vector quantization [6] and Grassmanian subspace packing [3]. In this paper the latter codebook is chosen with 32 elements (5-bit precision). Assigning \mathbf{W}_{32} the notation for the Grassmanian codebook with 32 elements,

$$\mathbf{q}_k^{LFBF} \triangleq \arg \min_{\mathbf{q}_k \in \mathbf{W}_{32}} \|\mathbf{q}_k - \mathbf{q}_k^{BF}\|_2 \quad (5)$$

and

$$\mathbf{g}_k^{LFBF} \triangleq \frac{\mathbf{H}_k \mathbf{q}_k}{\|\mathbf{H}_k \mathbf{q}_k\|_2} \quad (6)$$

using (4) above assuming that \mathbf{q}_k^{LFBF} approximates the dominant right singular vector of \mathbf{H}_k .

III. EXPERIMENT DESCRIPTION

The experiments conducted in this paper were designed to measure a variety of statistics and metrics of our system that provide insight into the feedback delay problem.

A. Prototype Setup and Indoor Wireless Channel

The experiments in this paper were performed in the indoor office environment depicted in Figure 3. The transmitter and receiver, separated by a distance of 10 m, are located in two cubicles as might be the case in typical indoor office usage. At a carrier frequency of 2.5 GHz, mobility is primarily determined by the motion of objects larger than 1×10^{-2} m. In the absence of movement in the environment, the wireless channel will remain static as the electromagnetic propagation in the environment does not change. The wireless channel in

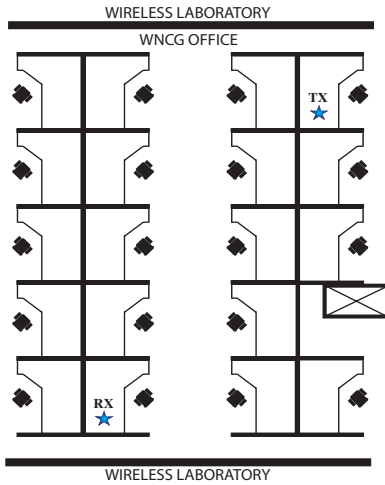


Fig. 3. Floor plan of indoor office setting for feedback beamforming experiment. The office has rows of cubicles, made with metal frames, and a large metal support column.

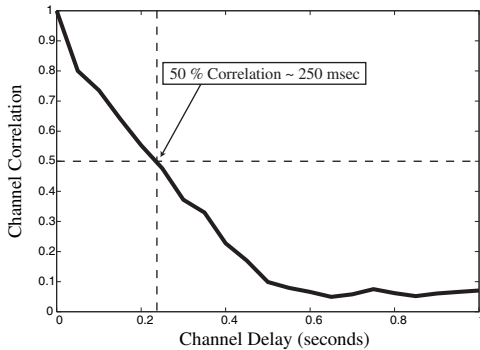


Fig. 4. Measured channel correlation statistics for indoor wireless channel. Coherence time is approximately 250 msec.

such a static environment remains highly correlated for hundreds of seconds, as verified through measurement in an empty office. To produce meaningful results, it is necessary to create a fading channel with stationary (or at least nearly stationary) correlation statistics. In order to create such a fading channel the antennas of each node were mounted on oscillating fans (on the body of the fan, not on the rotating blades). The two fans used in this experiment oscillated with periods of 13.75 seconds and 11.25 seconds respectively. This approach was necessary since moving large objects around the office to create the desired Doppler effect was not feasible.

Measuring correlation statistics using the fading channel mentioned required gathering channel measurements. Channel sounding was performed using repeated transmission of null packets (i.e. packets containing only the IEEE 802.11n training sequence and header). The correlation statistics computed from this data, shown in Figure 4, indicates that the coherence time of our indoor office setting is approximately 250 msec. This corresponds to other indoor wireless channel measurements in the literature [13].

B. Experiment Procedure

This experiment was conducted using a low-latency and error-free wired feedback channel implemented over a TCP/IP connection between the transmitter and receiver. Special care was taken to ensure that feedback delay was accurately produced and that CSI contained minimal estimation error. The procedure used in conducting the feedback experiments for this paper is described below.

- P0:** Pick a transmit power P_{TX} as a random number with uniform distribution $P_{TX} \sim \mathcal{U}[P_{TX_{min}}, P_{TX_{max}}]$.
- P1:** Transmit a packet using CDD, i.e. without feedback at transmit power P_{TX} for baseline comparison.
- P2:** Wait for 50 msec to allow receive processing to complete.
- P3:** Transmit a sounding packet at maximum transmit power to reduce estimation error in the estimate of the full MIMO channel.
- P4:** Wait for desired delay minus some ϵ time to account for processing delay and properly age feedback information.
- P5:** Transmit a packet using beamforming at transmit power P_{TX} . The beamforming vector is generated using CSI obtained over the wired feedback channel.
- P6:** Repeat steps **P4** and **P5** for additional feedback delays.
- P7:** Repeat steps **P0-P6** as needed to achieve desired precision in BER statistics over SNR range of interest.

The procedure above was performed for a variety of coding and modulation schemes. For each data rate, the impact of feedback delay can be measured effectively only over a specific SNR range. Capacity vanishes below this range, and BER becomes very small above this range. As such, $P_{TX_{min}}$ and $P_{TX_{max}}$ are tuned appropriately for each data rate to ensure operation in the desired SNR range. It is important to note that even though beamforming packets have variable transmit power, sounding packets are always transmitted at the maximum transmit power in the linear region of the transmit amplifier. This reduces the chance that channel estimation error adversely impacts beamforming.

After this procedure (i.e. sounding, wired feedback over TCP/IP, and feedback aging), the transmitter can use the uncompressed MIMO CSI to compute optimal beamforming vectors, or quantize it and then compute limited feedback beamforming vectors which are then used in the transmission of step **P5**. In the case where feedback is not available due to a dropped sounding packet (usually because of synchronization error), all subsequent packets will be sent using CDD until new feedback becomes available.

IV. RESULTS AND ANALYSIS

This section presents both the results and analysis of limited feedback beamforming and CSI delay experiments. These experiments use the physical layer algorithms of Section II and the setup procedure in Section III.

A. Throughput Gain Results

Previous theoretical analysis has shown that, under certain channel assumptions, there exists an upper bound on the capacity gain, $\Delta C(D)$, that limited-feedback beamforming provides (versus capacity of transmitter without CSI). Explicitly,

$$\Delta C(D) \triangleq C_{BF}(D) - C_{UI} \quad (7)$$

for uniformed transmitter capacity C_{UI} and limited feedback beamforming capacity C_{BF} as a function of delay D . Unfortunately, system capacity is not necessarily easily translated into realizable system performance. Past work has shown that, for a fixed bit-error-rate, QAM constellations exhibit a constant SNR (in dB) gap from capacity [19]. Therefore, by transmitting QAM constellations and selecting the proper constellation order and convolutional coding rate, it is possible to maintain a relatively static bit error rate and thus, approximate the capacity trend. Since the capacity of the wireless channel in this experiment is unknown, we measure the impact of feedback delay by observing the throughput of limited feedback beamforming and cyclic delay diversity. For a single spatial stream, the modulation and coding schemes (MCS) 0-7 in IEEE 802.11n provide rates of 0.5 to 5.0 Mbps in the Hydra physical layer. For the IEEE 802.11n physical layer we define throughput as

$$\mathcal{T}_{MCS,i}(\text{SNR}) \triangleq \mathcal{R}_i(1 - \text{BER}_i(\text{SNR})) \quad (8)$$

where \mathcal{R}_i , BER_i are the total rate and bit error rate for MCS i , respectively. Using this definition of throughput we further define *throughput gain*, $\Delta T(D)$, for limited-feedback beamforming as,

$$\Delta T(D) \triangleq \mathcal{T}_{BF}(D) - \mathcal{T}_{CDD} \quad (9)$$

for limited-feedback beamforming throughput \mathcal{T}_{BF} and cyclic delay diversity throughput \mathcal{T}_{CDD} . Cyclic delay diversity is used as a baseline comparison for uninformed transmission. Cyclic delay diversity provides full diversity order without any additional receiver processing. Using the frequency domain spatial mapping framework from Section II it is shown that cyclic delay diversity is a special case of transmit beamforming.

The bit-errors in each MCS were measured for 1000 packets over a range of SNR that covered the transition regions of the throughput curve. This results in a scatter plot of bit-errors per packet versus SNR measured from the extended training. An example for MCS 4 (16-QAM) can be observed in Figure 5. The SNR values were binned to small intervals and the BER was averaged over each bin. This BER versus SNR curve for MCS i was translated into throughput using equation (8). Through visual inspection, the correct SNR regions were observed for each MCS. Finally, to make the first and second order derivatives of the throughput function continuous, a cubic splines interpolation procedure was processed over the data. Figure 6 demonstrates the throughput calculation for limited feedback beamforming in a 5-bit codebook with 50 msec feedback delay and cyclic delay diversity.

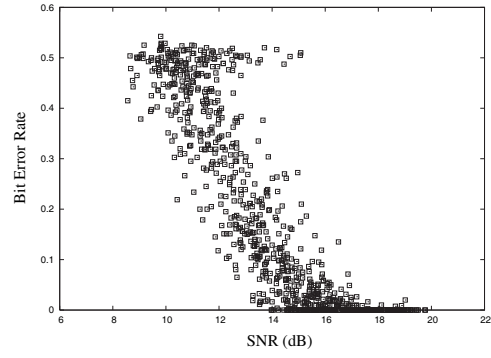


Fig. 5. Scatter plot of MCS 4 of experimental data

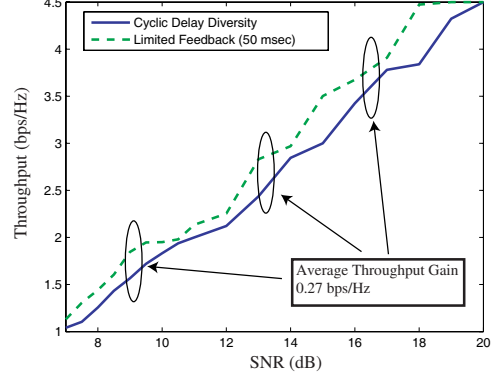


Fig. 6. Throughput versus SNR for limited feedback beamforming with 50 msec feedback delay and cyclic delay diversity

Throughput curves were generated for 100 – 1000 msec feedback delay over all the MCS. In order to compare with theoretical feedback delay effects from [11], the throughput gain was calculated using (9) as an approximation of (7). The resulting throughput calculations are displayed in Figure 7. Also included in this graph, and as discussed in detail in the next subsection, is the theoretical upper bound from [11].

B. Performance Analysis

Figure 6 observes the throughput gain of limited feedback with 50 msec delay versus cyclic delay diversity for a baseline comparison. As expected, limited feedback beamforming im-

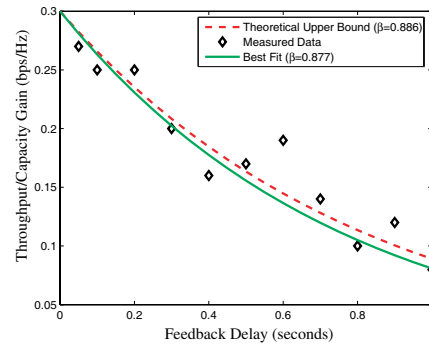


Fig. 7. Throughput gain versus feedback delay for limiting feedback beamforming and 5-bit codebooks

proves the performance of the system over all SNR. Since the coherence time of the wireless channel was observed to be approximately 250 msec, a 50 msec delay should be very close to the maximum achievable throughput gain. The throughput gain is averaged over 7 – 22 dB SNR to yield 0.27 bps/Hz. Experimental results display degraded performance likely as a result of impairments not observed in typical wireless channel models. This can include frequency offset, synchronization error, phase noise, channel estimation error, and nonlinearities in hardware components.

The principle contribution of this experiment is shown in Figure 7. This figure displays the loss in throughput versus feedback delay. Analytical results from [11] show that the capacity gain as a function of feedback delay can be bounded by an exponential function. Specifically,

$$0 \leq \Delta C(D) \leq \alpha \beta^D \quad (10)$$

for scalar constants $\alpha, \beta \in \mathbb{R}$ and $D \in \mathbb{N}$ the normalized delay. D is the number of state transitions taken in a Markov process that models the temporal correlation of the wireless channel. α refers to the capacity gain of limited feedback beamforming with zero feedback delay. β is the second largest eigenvalue of the transition probability matrix which describes the evolution of the wireless channel through quantized codebook space. For example in our limited feedback beamforming experiment, we measure the state of the channel every 50 msec. Each 50 msec step corresponds to an increment of D . The transition probability matrix corresponds to the conditional probability that the quantized limited feedback beamforming vector switches between any two codebook indices.

In Figure 7, the measured data represents the observed throughput gain as a function of feedback delay. Using an exponential fit to the measured data with $\alpha = 0.3$, the least squares solution for the exponential term yields $\beta = 0.877$. Additionally, by collecting statistics on the transitions of the indices of the quantized codebook we were able to reconstruct the transition probability matrix. This transition probability matrix provides $\beta = 0.886$ from the 2nd largest absolute eigenvalue. Therefore, we have two results that characterize capacity (throughput) gain as an exponential function of the feedback delay. The first result was obtained through exhaustive throughput measurements over various SNR, feedback delay, and MCS. The second result, however, only required collecting statistics at a single SNR and feedback delay (50 msec) to compute the transition probability matrix. Although the second result theoretically represents an upper bound on the capacity (throughput) gain as a function of delay, this upper bound accurately approximates the capacity (throughput) gain that we observed.

V. CONCLUSION

In this work we have characterized the impact of feedback delay on the performance of limited feedback beamforming through measurements in real wireless channels. These measurements were obtained on a IEEE 802.11n draft 2.0 standard MIMO-OFDM prototype. The measurement of throughput

gain versus feedback delay in this experiment verifies the accuracy of analytically derived performance bounds [11]. Furthermore, verifying these results suggests a simple procedure to characterize the performance of feedback delay in limited feedback beamforming without exhaustive throughput measurements.

REFERENCES

- [1] T. K. Y. Lo, "Maximum Ratio Transmission," *IEEE Trans. on Communications*, vol. 47, pp. 1458–1461, October 1999.
- [2] D. J. Love, R. W. Heath, Jr., W. Santipach, and M. L. Honig, "What Is the Value of Limited Feedback for MIMO Channels?" *IEEE Communications Magazine*, vol. 42, pp. 54–59, October 2004.
- [3] D. J. Love, R. W. Heath, Jr., and T. Strohmer, "Grassmannian Beamforming for Multiple-Input Multiple-Output Wireless Systems," *IEEE Trans. on Info. Theory*, vol. 49, pp. 2735–2747, October 2003.
- [4] K. K. Mukkavilli, A. Sabharwal, E. Erkip, and B. Aazhang, "On Beamforming With Finite Rate Feedback in Multiple-Antenna Systems," *IEEE Trans. on Info. Theory*, vol. 10, pp. 2562–2579, October 2003.
- [5] V. K. N. Lau, Y. Liu, and T.-A. Chen, "Optimal Partial Feedback Design for MIMO Block Fading Channels with Feedback Capacity Constraint," in *IEEE International Symposium on Information Theory*, June 2003, p. 65.
- [6] B. Mondal and R. W. Heath, Jr., "Performance Analysis of Quantized Beamforming MIMO Systems," *IEEE Transactions on Signal Processing*, vol. 54, pp. 4753–4766, December 2006.
- [7] A. Hottinen, R. Wichman, and O. Tirkkonen, *Multi-Antenna Transceiver Techniques for 3g and Beyond*. New York, NY, USA: John Wiley & Sons, Inc., 2003.
- [8] J. Du, Y. Li, D. Gu, A. F. Molisch, and J. Zhang, "Estimation of Performance Loss Due to Delay in Channel Feedback in MIMO Systems," in *Proceedings of IEEE Vehicular Technology Conference 2004*, vol. 3, September 2004, pp. 1619–1622.
- [9] D. Li and X. Dai, "On the performance of MIMO-OFDM Beamforming Systems with Feedback Delay," in *International Conference on Wireless Communications, Networking and Mobile Computing*, September 2006, pp. 1–4.
- [10] E. Au, S. Jin, M. McKay, W. H. Mow, X. Gao, and I. Collings, "Analytical performance of mimo-svd systems in rician fading channels with channel estimation error and feedback delay," *Wireless Communications, IEEE Transactions on*, vol. 7, no. 4, pp. 1315–1325, April 2008.
- [11] K. Huang, B. Mondal, R. W. Heath, Jr., and J. G. Andrews, "Effect of Feedback Delay on Multiple-Antenna Limited Feedback for Temporally-Correlated Channels," in *Proceedings of IEEE Global Telecommunications Conference*, October 2006, pp. 1–5.
- [12] K. Mandke, S.-H. Choi, G. Kim, R. Grant, R. C. Daniels, W. Kim, S. M. Nettles, and R. W. Heath, Jr., "Early Results on Hydra: A Flexible MAC/PHY Multihop Testbed," in *Proceedings of the 65th IEEE Vehicular Technology Conference*, Apr. 2007, pp. 1896–1900.
- [13] K. Mandke, R. C. Daniels, S.-H. Choi, S. M. Nettles, and R. W. Heath, Jr., "Physical Concerns for Cross-Layer Prototyping and Wireless Network Experimentation," in *Proceedings of the Second ACM International Workshop on Wireless Network Testbeds, Experimental Evaluation and Characterization*, 2007.
- [14] "Hydra: A mimo-ofdm multihop wireless network prototype." [Online]. Available: <http://hydra.ece.utexas.edu>
- [15] A. Paulraj, R. Nabar, and D. Gore, *Introduction to Space-Time Wireless Communications*. Cambridge University Press, 2003.
- [16] *Wireless LAN Medium Access Control (MAC) and Physical Layer (PHY) Specifications - Draft 2.0: Enhancements for Higher Throughput*, Part 11 standard ed., IEEE 802.11n Working Group, February 2007.
- [17] A. Dammann and S. Kaiser, "Standard conformable antenna diversity techniques for OFDM and its application to the DVB-T system," in *IEEE Global Telecommunications Conference*, vol. 5, 2001, pp. 3100–3105 vol.5.
- [18] G. Bauch, "Capacity optimization of cyclic delay diversity," in *IEEE Vehicular Technology Conference*, vol. 3, 2004, pp. 1820–1824 Vol. 3.
- [19] J. Cioffi, *Digital Communications*. Stanford University Course Reader, 2006.